Available online at www.sciencedirect.com
ScienceDirect
Trans. Nonferrous Met. Soc. China 32(2022) 908−926
Transactions of Nonferrous Metals Society of China
www.tnmsc.cn

Role of interlayer composition in microstructure and mechanical properties during TLP bonding of GTD-111/IN-718 superalloys

Ali IZADI GHAHFEROKHI[1], Masoud KASIRI-ASGARANI[1],
Kamran AMINI[2], Mahdi RAFIEI[1], Reza EBRAHIMI-KAHRIZSANGI[1]

1. Advanced Materials Research Center, Department of Materials Engineering, Najafabad Branch, Islamic Azad University, Najafabad, Iran;
2. Center for Advanced Engineering Research, Majlesi Branch, Islamic Azad University, Isfahan, Iran

Received 21 March 2021; accepted 10 September 2021

Abstract: An investigation was carried out to assess the applicability of transient liquid phase bonding of two dissimilar super-alloys with different interlayers. The effect of using three types of interlayer such as BNi-2, BNi-3, and BNi-9 on microstructure and mechanical properties was studied in the GTD-111/IN-718 system at 1100 °C for different bonding time. To determine the compositional changes and microstructure in the joint region, field emission scanning electron microscopy equipped with energy dispersive spectroscopy was utilized. The formation of Ni_3B in the athermally solidified zone (ASZ) is controlled by the B content and, accordingly, the morphology of Ni_3Si is governed by the Si content. The Cr content might impede the relocation of B from the interlayer into the base metal and the formation of CrB inside the ASZ is dominated by the Cr content. The high micro-hardness of the eutectic compounds is originated from the formation of boride matrixes such as Ni or Cr boride. The shear strength of the joint using BNi-9 after the completion of isothermal solidification is lower compared that that using BNi-3 and BNi-2, which could be related to the absence of Si in the filler metals constituent and the significant presence of Cr in BNi-9.
Key words: transient liquid phase bonding; Ni-based superalloy; isothermal solidification; Ni−B compounds

1 Introduction

Nickel-based super-alloys have many attractive specifications such as excellent high temperature tensile strength and good fatigue strength, microstructural stability, adequate creep, and stress rupture properties along with proper corrosion and oxidation resistance [1]. The use of nickel-based super-alloys as a very important group of materials in most industries is due to the high concentration of the alloy element solubility, the existence of a corrosion resistant layer with the supplementary Al and Cr elements, and the enhancement of mechanical properties as well as the creep behavior by γ' and γ'' intermetallic phases with the addition of Al, Nb, and Ti. The presence of Ni enhances the stress corrosion cracking (SCC) resistance in some corrosion environments [2]. Due to these interesting characteristics, nickel-based super-alloys are used for manufacturing components in the hot section of power turbines and aircraft engines [3]. However, because of the exposure of these alloys to high temperatures, they are prone to degradation and it is more efficient to repair damage instead of full replacement of the parts. One of the most popular repair methods in the world is welding [4], although it is often recognized as an unsuitable method for bonding nickel-based super-alloys due to their high sensitivity to both hot

Corresponding author: Masoud KASIRI-ASGARANI, E-mail: m.kasiri.a@gmail.com, m.kasiri@pmt.iaun.ac.ir;
Kamran AMINI, E-mail: kamran_amini1978@hotmail.com, k.amini@iaumajlesi.ac.ir
DOI: 10.1016/S1003-6326(22)65842-4

cracking during welding and post-weld heat treatment cracking [5]. Hence, a combination of diffusion bonding and brazing techniques known as the transient liquid phase (TLP) method is a superior choice for joining/repairing of Ni-based super-alloys [6]. The TLP process involves the insertion of a filler metal with a composition similar to that of the base metals. The filler metal usually contains the melting point depressant (MPD) elements such as B and Si. With the heating of the assembly containing two base metals and a filler metal between them up to the bonding temperature that is higher than the filler melting point and lower than the base metal melting point, the filler material melts. The parts that are the nearest to the joint region of the substrates dissolve and the solid/liquid interface starts to move during the melting of the filler material. Then, the molten zone is developed up to a local equilibrium at liquid/solid interface. The MPD elements such as B and Si diffuse into the base metal and exchange with the chemical composition of the interface and increase its melting point. Isothermal solidification starts with increasing the melting point over the temperature of the joint area. The solid/liquid interface moves in the direction of the joint center and isothermal solidification will be completed. By TLP bonding, we could achieve joints with appropriate microstructure and mechanical properties [7]. Several studies have applied the TLP bonding method to join the Ni-based alloys and then investigated the microstructural and mechanical properties of the joint. For example, BAKHTIARI et al [8] studied the mechanical properties of IN738/MBF20/IN718 system based on the repair process of the related gas turbine components. GHAHFEROKHI et al [9] reported the microstructural and mechanical properties of GTD-111 and IN-718 by the BNi-9 interlayer joined via dissimilar TLP bonding. Also, to accomplish appropriate joints, some research projects have focused on the effect of the chemical composition of different interlayers on TLP micro-structure. For example, POURANVARI [10] studied the influence of the filler type on the shear strength and microstructural characteristics of the joints. YUAN et al [11] reviewed the effect of boron and silicon on microstructure and isothermal solidification through TLP bonding of duplex stainless steel using different filler alloys. The effect of configuration and composition of the interlayer on the TLP joints of FSX-414 super-alloy has been reported by BAKHTIARI [12]. RABINKIN [13] investigated the characteristics of amorphous brazing foil and surveyed the positive qualities it has brought to several applications.

GTD-111 Ni-based super-alloys developed by General Electric Company used as a blade material of land-based gas turbines are γ-prime strengthened nickel-based super-alloys which are widely used in gas turbines and the hot section of aero-engines. These super-alloys have superior properties at high temperature such as outstanding tensile strength and microstructural stability, good fatigue strength, satisfactory creep and stress rupture properties along with proper oxidation and corrosion resistance [1]. IN-718, which was developed by International Nickel Company in the 1950s [14], is a strengthened super-alloy and is one of the suitable materials widely used for space applications and critical aero-engines. These super-alloys have superior properties such as high temperature and creep-resistant applications [15].

One of the important methods for manufacturing and repairing similar (GTD-111 or IN-718) and dissimilar (GTD-111/IN-718) structure materials is the TLP bonding. According to a previous investigation, the dissimilar joining of GTD-111 and IN-718 was carried out by TLP bonding [9]. In the case of similar joining, microstructural evolution of high-performance Ni-based super-alloy GTD-111 by SAJJADI et al [16] and the influence of microstructural development on mechanical properties of diffusion brazed IN718/BNi-2/IN718 [17] have been reviewed. In the case of dissimilar joining, the dissimilar TLP bonding of IN-718/IN-738 alloy and In600/In600 alloy jointed with Nicobraz 150 interlayer was studied by EGBEWANDE et al [18]. They showed that faster isothermal solidification happens in the In738 side, which is due to the existence of some elements with a greater tendency to react with B and intermetallic compounds formed in the IN-738 alloy. Microstructure of dissimilar TLP joints of IN-738/MBF20/IN-718 was evaluated at different bonding temperatures [19]. In the above-mentioned study, the dissolution of the base metals in the melt joint area was recognized as the most important reason for remaining the athermal solidification zone (ASZ) in the joint centerline with higher

bonding temperature and longer bonding time.

In this study, TLP bonding of GTD-111/IN-718 system was assessed using different Ni-based interlayers (BNi-2 and BNi-3 with the MPD elements of B and Si), and BNi-9 with B as the MPD element for investigating the effect of the interlayer composition and bonding time on the microstructure and mechanical properties of the TLP joint. The effects of boron, silicon, and chromium on the microstructure, hardness and shear strength of the joint are the specific interests of this study. The presence of different amounts of the above-mentioned elements in different filler alloys such as BNi-2, BNi-3, and BNi-9 can affect the microstructure and mechanical properties of the joints.

2 Experimental

2.1 Methods

The composition of the B−Ni compounds such as BNi-2, BNi-3 and, BNi-9 filler metals (obtained from Metglas, Hitachi Metals Trading Ltd., Tokyo, Japan) in the form of amorphous foils with 50 μm in thickness is given in Table 1. The joining metal specimens were machined to dimensions of 10 mm × 10 mm × 5 mm using wire-cutting machine. The joining surfaces were ground using the grit sizes of No. 60−1500 SiC emery papers. The samples were cleaned for 15 min in an acetone ultrasonic bath followed by the TLP bonding process in a vacuum furnace with the applied bonding pressure of 1.33×10^{-2} Pa. The thickness of the amorphous foils used for the interlayer was 50 μm. The bonded samples were prepared metallographically (perpendicularly sectioned to the bond) and the sectioned specimens were ground using the grit sizes of No. 80−3000 SiC paper. After that, the specimens were polished by disc polishing using Al_2O_3 solution so as to achieve a mirror finish of 1 μm on the welds. After metallographic preparation, the specimens were studied using field emission scanning electron microscopy (FE-SEM) equipped with energy-dispersive spectrometry (EDS) and X-ray diffraction (XRD) analysis. The bonding was developed at 1100 °C for 1, 15, 30, 45, 60 and 90 min. The heating rate was 10 °C/min, and it was then furnace-cooled to room temperature. A schematic fixture for fixing of the samples during TLP bonding process is shown in Fig. 1(a). Two different etchants were used in order to study microstructural properties. In order to show the precipitates adjacent to the interlayer/base metal interface, Murakami etchant (10 g KOH, 10 g $K_3[Fe(CN)_6]$, 100 mL H_2O) was used, which favorably etches the Cr-rich phases. Moreover, the

Table 1 Chemical composition of base metals and interlayers (wt.%)

Material	Ni	Cr	Co	Ti	Al	W	Mo	Ta	Fe	Nb	C	B	Si
GTD-111	Bal.	13.5	9.5	4.75	3.3	3.8	1.53	2.7	0.23	–	0.09	0.01	–
IN-718	Bal.	18	0.06	0.92	0.4	–	3.3	0.05	17.86	4.41	0.03	0.007	–
BNi-2 (Metglas)	Bal.	7.0	–	–	–	–	–	–	3.0	–	–	3.2	4.5
BNi-3 (Metglas)	Bal.	–	–	–	–	–	–	–	–	–	–	3.2	4.5
BNi-9 (Metglas)	Bal.	15	–	–	–	–	–	–	–	–	–	4.0	–

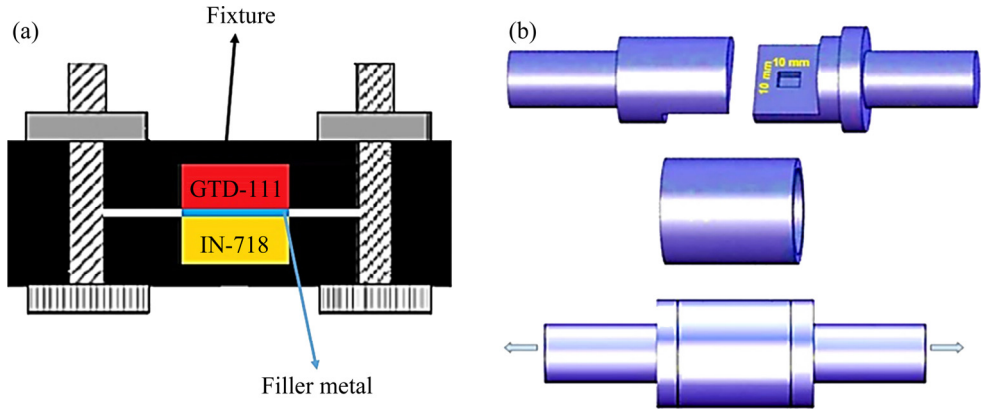

Fig. 1 Schematic of fixtures: (a) Fixture for fixing samples during TLP bonding; (b) Shear test fixture [20]

$\gamma-\gamma'$ microstructure of the isothermally brazed joints was recognized by applying the Kalling's reagent (1.5 g $CuCl_2$ + 33 mL ethanol + 33 mL H_2O + 33 mL HCl) which favorably etches the γ phase. FE-SEM (FEI-QUANTA FEG450) was employed to investigate the microstructure of the bonding region and EDS was used to determine the chemical composition. The XRD patterns were obtained using the PHILIPS PW3040 diffracto-meter with a wavelength 1.54 Å in order to specify the phases in the fracture surface. Mechanical properties were evaluated by using the hardness and shear strength tests. Vickers micro-hardness test was performed according to the ASTM E384 standard for the hardness profiling of the bonding zone. The test was performed on a cross-section of specimens with a load of 0.196 N using a Buehler machine.

The shear strength test was performed as per the ASTM D1002 standard using a Zwick/Roell tensile machine with a cross-head speed of 1 mm/min. A D3 tool steel fixture was designed for the shear testing of the bonded coupons and holding the assembly during the tensile test, as it is schematically shown in Fig. 1(b).

2.2 Materials

In this investigation, different Ni-based super-alloys, namely GTD-111 and IN-718 (obtained from Western Australian Specialty Alloys Pty Ltd.), were selected in the form of sheets with 5 mm in thickness and the compositions defined in Table 1. Figures 2(a, c) show the microstructure of GTD-111 and IN-718 base metals, respectively. The GTD-111 microstructure was composed of a γ solid solution as the matrix accompanied by finely dispersed γ' precipitates. Throughout the solidification process, carbides and $\gamma-\gamma'$ eutectic islands were formed in the microstructure. Because of the precipitation of large γ' particles near the grain boundaries as a result of the unusual movement of the grain boundaries, the presence of serrated grain boundaries can be seen in the microstructure presented in Fig. 2(a) [21]. The (Ta,W,Ti)C carbides are the most usual carbides which are formed during the solidification of the GTD-111 alloy [22]. The IN-718 microstructure consisted of γ' precipitates and γ'' precipitates in the matrix of γ (Fig. 2(c)). During the solidification process, carbides and delta phases were created on the grain boundaries. The XRD results presented in Figs. 2(b, d) confirm the phases recognized in the SEM images. The strengthening elements in the Ni-based super-alloy such as IN-718 and GTD-111 are mainly Nb, Al, and Ti elements. The tensile strength of GTD-111 is approximately 870 MPa at room

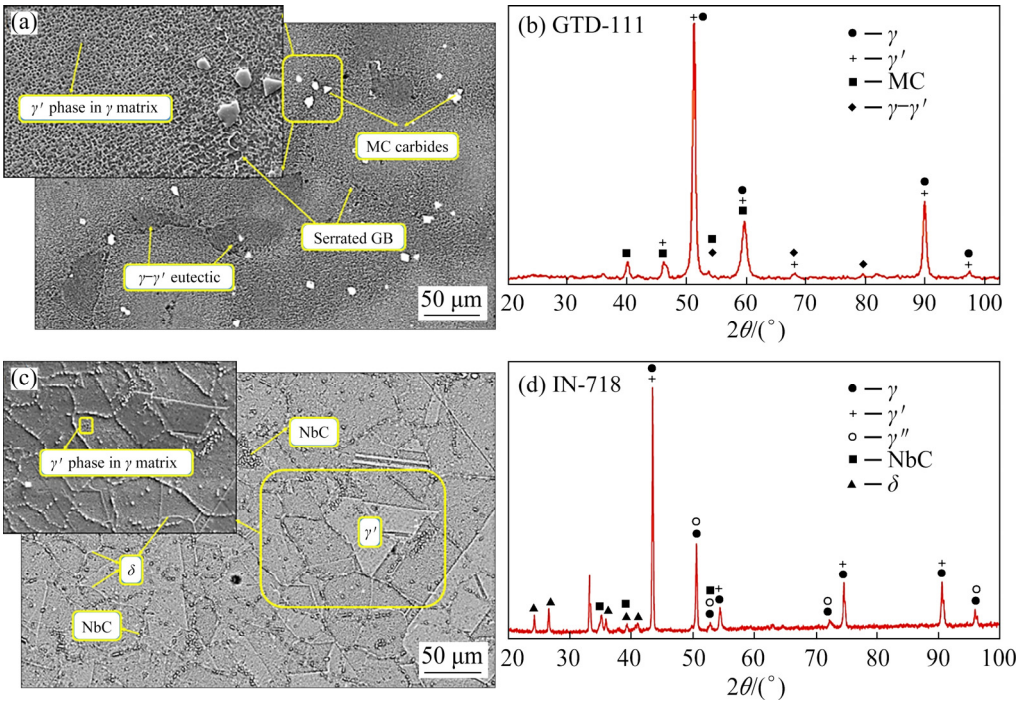

Fig. 2 Microstructures of base metals: (a) FE-SEM image illustrating microstructure of GTD-111; (b) XRD pattern of GTD-111; (c) FE-SEM image illustrating microstructure of IN-718; (d) XRD pattern of IN-718

temperature and 510 MPa at 1100 °C. The tensile strength of IN-718 is approximately 790 MPa at room temperature and 450 MPa at 1100 °C. Mechanical properties of GTD-111 and IN718 were reported by SAJJADI et al [23] and LEE et al [24], respectively.

3 Results and discussion

3.1 Microstructure of joint

A typical TLP microstructure of the GTD-111/IN-718 system with BNi-2 interlayer made at a bonding temperature of 1100 °C with a holding time of 45 min is shows in Fig. 3. Different distinct zones that are visible in this image include the isothermal solidification zone (ISZ), athermal solidification zone (ASZ) [25], diffusion affected zone (DAZ), and finally different base metals (BM) containing GTD-111 and IN-718. The principal cause for the melting of the interlayer and the occurrence of important inter-diffusion between the interlayer and base metal is the lower melting point of the interlayer compared with the bonding temperature.

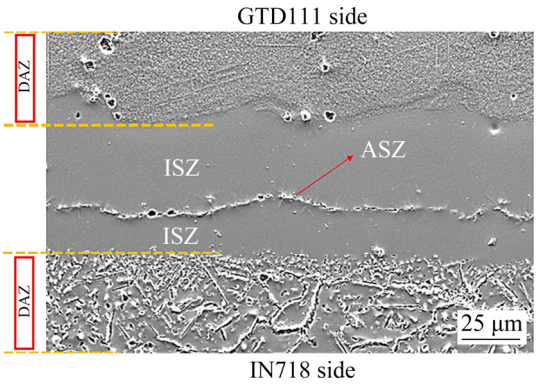

Fig. 3 FE-SEM image illustrating microstructure of joint region using BNi-2 filler alloy at 1100 °C for bonding time of 45 min

In other words, as the bonding temperature (i.e., 1100 °C) is higher than liquidus temperature of the interlayers (i.e., 1026, 1065, 1082 °C for BNi-2, BNi-3, and BNi-9, respectively), the interlayer melts.

The solidification phenomena contain two modes: (1) Mode I is the isothermal solidification; (2) Mode II is the athermal solidification.

The driving force for isothermal solidification is the compositional change from inter-diffusion of the alloying elements between the base metal and the filler metal at a constant temperature during the holding time. Isothermal solidification starts and causes the liquidus temperature to reach the bonding temperature (T_B). The melting temperatures of the interlayers obtained using differential scanning calorimetry (DSC) are schematically shown in Fig. 4. The liquidus temperature of the BNi-2, BNi-3, and BNi-9 filler metals reported by several researchers [13,26,27] is lower than the bonding temperature of 1100 °C. The reason for choosing the bonding temperature of 1100 °C is to ensure that all three layers are liquid at the bonding temperature. BAKHTIARI [12] selected a bonding temperature of 1150 °C for bonding with three different interlayers of MBF-60, MBF-80, and MBF-100. POURANVARI [10] reported bonding at 1100 °C using three different interlayers of BNi-2, BNi-3, and BNi-9. Therefore, interlayer melting is assured at 1100 °C. The chemical composition changes of the liquid phase swirl the liquidus temperature. The main indicator for the effect of the alloying elements on the liquidus temperature is the distribution coefficient (K) [28]. Increasing the liquidus temperature of the liquid phase helps us with two phenomena: (1) Emptying of the liquid phase from elements with K value less than unity, such as the MPD elements, causes the raising of the liquidus temperature of the liquid phase. (2) The presence of elements with K value larger than unity, such as Cr and Fe in the liquid, shows the dissolution of the base metal and Cr and Fe diffusion from the base metal into the bond area during the bonding process,

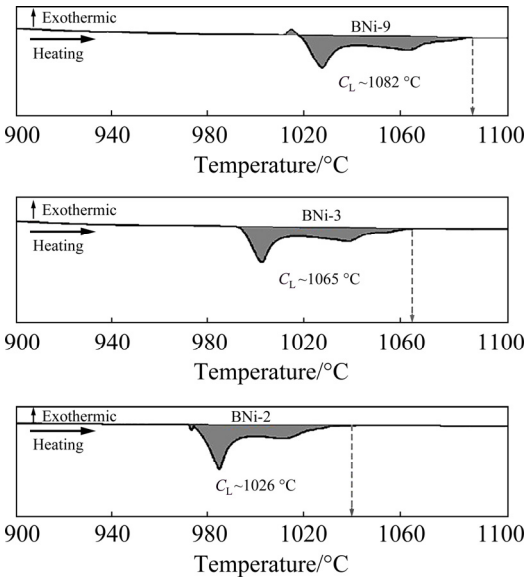

Fig. 4 DSC heating traces of BNi-2, BNi-3, and BNi-9 filler metals

which will cause the raising of liquidus temperature of the liquid phase. With the adjustment of the bonding time, the isothermal solidification can be achieved at a constant temperature.

The driving force for athermal solidification is the cooling presses. Microstructure of the ASZ in the joint obtained with increasing the Cr content in the filler using BNi-9 contained γ-Ni, Ni_3B and Cr borides. With increasing the Si content in the interlayer, Ni_3Si remained in the joint centerline using BNi-3. The Cr content in the interlayer affected the completion of isothermal solidification process. As can be seen, in athermal solidification conducted at 1100 °C by using BNi-9 instead of BNi-3, the increased Cr in the filler metal formed a joint with ternary eutectic phases along the centerline region after holding for a similar time. The Cr element could postpone the moving of B from the interlayer to the base metal [29]. The formation mechanism of microstructural changes in the bond centerline in the ASZ and in the interface is described below.

3.1.1 Microstructure of joint using BNi-2 filler alloy

Microstructure of the TLP bonded GTD-111 and IN-718 super-alloy at 1100 °C using the BNi-2 filler alloy with 50 μm in thickness and bonding time of 1 min is shown in Fig. 5. The existence of a

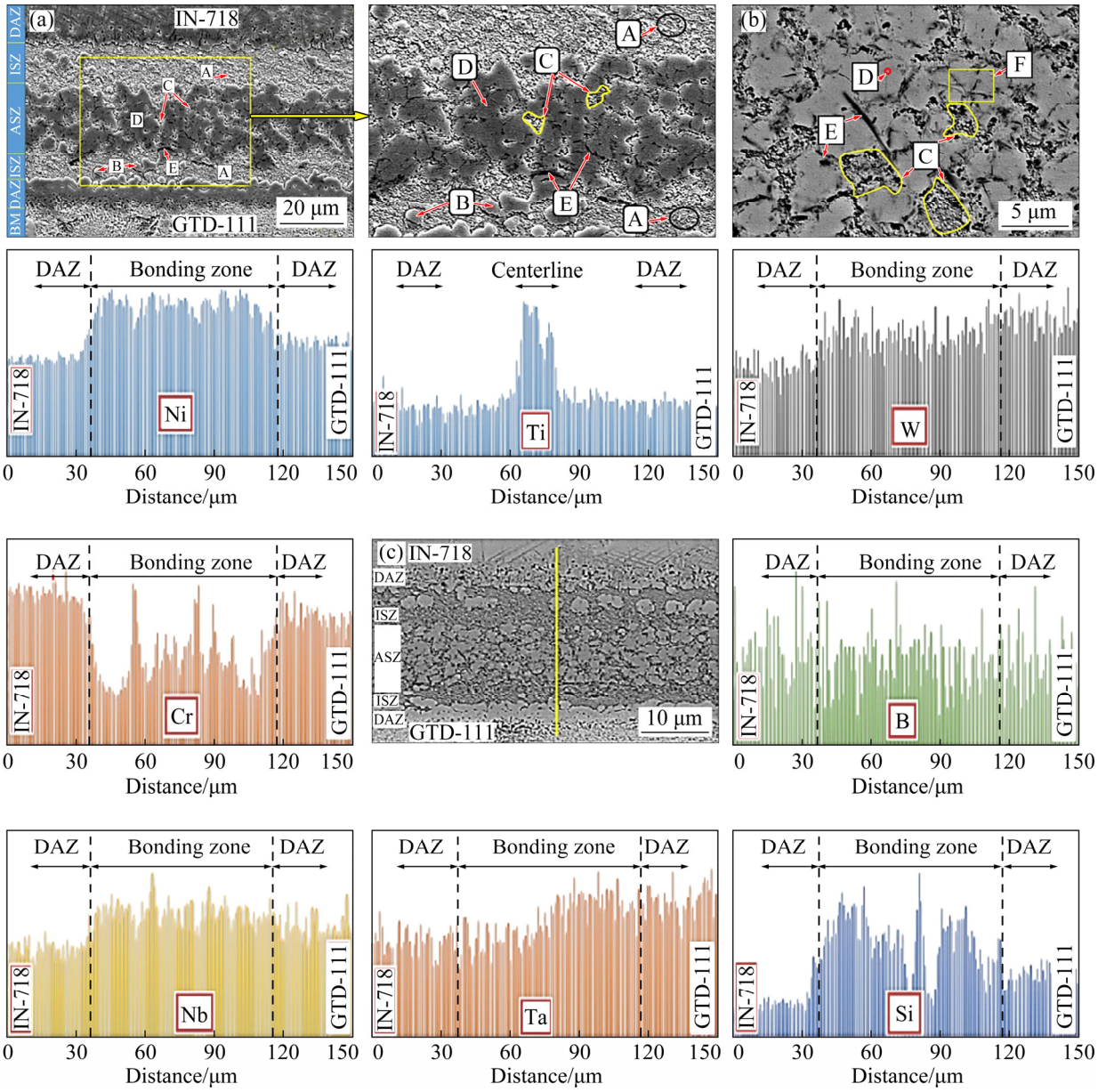

Fig. 5 SEM−EDS analysis results of typical cross-section made using BNi-2 at 1100 °C for 1 min: (a) Overview morphology; (b) Magnified backscatter morphology; (c) EDS line scan from joint region

comprehensive joint with good wettability is completely visible. The image reveals that 1 min bonding time was not adequate to complete the isothermal solidification and non-isothermal solidification caused eutectic compounds to form at the centerline of the joint. From SEM−EDS analysis, the following considerations could be given concerning Zones A−F designated in Figs. 5 and 6.

(1) As shown in Fig. 5(a), Zone A is a Ni-rich solid solution formed because of the isothermal solidification process. The presence of the alloy elements such as Nb, Ta, Ti, Al, Co and Fe which do not originally exist in the chemical composition of the filler alloy indicates the dissolution of base metals. According to the EDS results given in Table 2, the ISZ contains a higher amount of Ni but low amount of Nb, Ta, Ti, Al, Co, and Fe compared with the base metals. The B content was not detected in the ISZ although according to the EDS analysis the Si content develops in the ISZ because of its low diffusion coefficient in contrast to the boron. As can be seen in Fig. 6, a flower-shaped morphology is observable in ISZ which is composed of Ni-rich solid solution (Figs. 6(a, b)). Also, some granular particles containing Ni_3Si precipitates are observed in the residual melt adjacent to ASZ (Figs. 6(c, d)).

(2) Zone B is Ni-rich boride formed through the cooling of the remaining liquid. In this zone, the presence of boron was also identified by the ultrathin window EDS detector. Although EDS is a semi-qualified method for the detection of the boron element, there is a limitation in quantitative detecting of the light elements. Due to the solidification of the nickel-based alloys, segregation of Nb and Ta elements into the Ni-rich borides occurs (see Table 2).

(3) Zone C is composed of narrow eutectic micro-constituents made during the cooling of the remaining liquid. As can be seen in the EDS analysis, high silicon content was detected in this zone. Also, boron was recognized in this area. The combination of the EDS results and lamellar morphology indicates a ternary eutectic structure containing Ni−Si−B, similar to the solidification sequence results reported by ARAFIN et al [30].

(4) Zone D is a Ni-rich γ solid solution formed during athermal solidification of the remaining liquid as a part of the eutectic solidification product. This region consists of silicon content and no content of boron. Because of the non-solubility of silicon in the borides phase, the concentration of silicon increases in the γ solid solution.

(5) According to Fig. 5(b), Zone E is a Cr-rich boride formed during the cooling of the residual

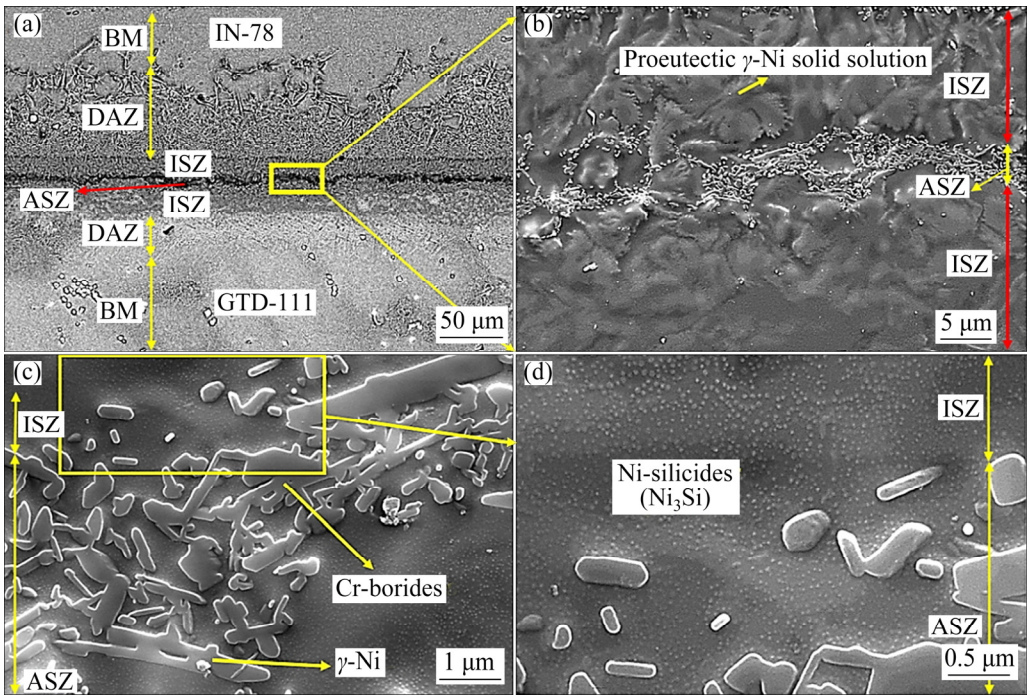

Fig. 6 FE-SEM images of bond prepared using BNi-2 at 1100 °C for 1 min: (a, b) Overview of joint centerline consisting of ISZ and ASZ; (c, d) Morphology of ASZ and its adjacent phases

Table 2 EDS analysis results of different areas in Fig. 5 (at.%)

Element	γ-solid solution (Zone A)		ASZ				
	ISZ in side of GTD-111	ISZ in side of IN-718	Ni-rich boride phase (Zone B)	Ternary eutectic (Zone C)	Ni-rich solid solution (Zone D)	Cr-rich boride (Zone E)	Ni-rich silicide (Zone F)
Ni	76.66	79.45	81.47	72.41	72.39	40.5	73.67
Cr	10.31	6.86	6.48	6.83	13.79	49.02	6.78
Fe	6.46	5.87	5.14	4.60	2.52	3.54	5.10
Nb	0.04	2.06	2.19	1.65	1.71	1.74	2.58
Ta	2.19	0.79	2.37	3.01	1.89	1.61	2.27
Si	0.00	0.69	0.03	8.84	6.09	0.22	6.28
Mo	0.84	1.22	1.12	0.72	0.75	1.59	0.03
Ti	0.73	0.53	0.47	0.87	0.36	0.71	0.72
Al	0.09	0.04	0.05	0.03	0.37	0.01	0.11

liquid. The high amount of chromium in this area and the simultaneous detection of boron in it suggest that this intermetallic phase is a Cr-rich boride.

(6) Zone F is a Ni-rich silicide. As can be seen in Figs. 5(c) and 6(b), the precipitates of Ni-rich silicide were observed in the Ni-rich solid solution adjacent to the boride phases. The morphology of these precipitates indicates that they were formed during the solid state precipitation reaction. As it was previously mentioned, a high concentration of Si was recognized from the EDS analysis. The EDS line scan from the joint region given under 1100 °C, 1 min condition using BNi-2 filler is shown in Fig. 5(c). For BNi-2, there are different results reported by several researchers. For example, RUIZ-VARGAS et al [26] identified four phases including α-Ni, γ'-Ni_3Si, Ni_3B, and CrB achieved by the slowly solidified BNi-2 specimens. On the other hand, LEBAILI and HAMAR-THIBAULT [31] identified three phases including α-Ni, Ni_3B and δ-Ni_6Si_2 with the solidification of the BNi-2 samples.

The XRD pattern from the surfaces of a fractured bond is presented in Fig. 7(a). The results reveal that Ni_3B, Ni_3Si, Ni_2B, and CrB are produced in the Ni matrix. Similar phases have also been reported by various researchers in their investigation of the TLP bonding of Ni-based super-alloys using different interlayers [20,32].

3.1.2 Microstructure of joint using BNi-3 filler alloy

Figure 8 displays SEM micrograph of a joint produced at 1100 °C for 1 min using the BNi-3 filler with 50 μm in thickness. The ISZ is composed of a Ni-rich solid solution layer which is formed at the solid/liquid interface towards the joint centerline because of the isothermal solidification process. EDS analysis results of the isothermal solidification zone is exhibited in Table 3. As it was previously mentioned, the phases with the B content were not detected in the ISZ, but due to low diffusion coefficient of Si compared with B, this phase somewhat tends to form in the ISZ.

According to the EDS results and SEM images, it could be claimed that ASZ was composed of three distinct phases marked by A, B, and C:

(1) Phase A is the eutectic structure containing the Ni−Si−B intermetallics. The elements of boron and silicon were recognized in the EDS point scan in this region (Fig. 8(a)). According to Table 3, this region contained a high silicon amount. Hence, this point can be considered Ni−Si−B intermetallics. Although the original composition of the BNi-3 filler alloy was free from the base alloying elements (such as Cr, Ti and Al), the dissolution of the base alloy in the liquid phase and inter-diffusion within the liquid and solid phases caused notable improvement of the liquid phase with the base alloying elements. The creation of various little borides in the bonding zone can be described by the simultaneous presence of the base alloying elements such as Cr and B in the remaining liquid phase and also the high similarity between these elements. However, this phase was not observed in the XRD pattern (Fig. 7(b)).

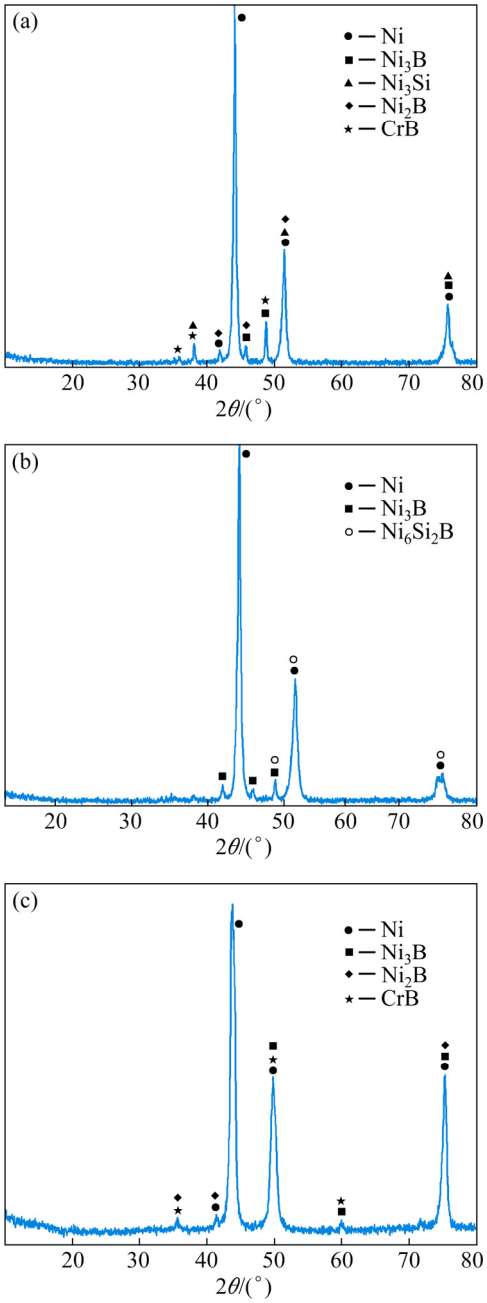

Fig. 7 XRD patterns of bonding region using different filler metals: (a) BNi-2; (b) BNi-3; (c) BNi-9

(2) Phase B is the Ni-rich boride formed during the cooling of the remaining liquid. Although boron was detected in the phase, its quantity could not be defined with sufficient exactness due to the X-ray absorption by EDS analyzer window. The EDS−SEM results of other components (Table 3) suggest that this phase is Ni-rich boride.

(3) Phase C is the Ni-rich silicide. Based on Figs. 8(b, c) and the EDS analysis (Table 3), an increase in Si content in the precipitation region

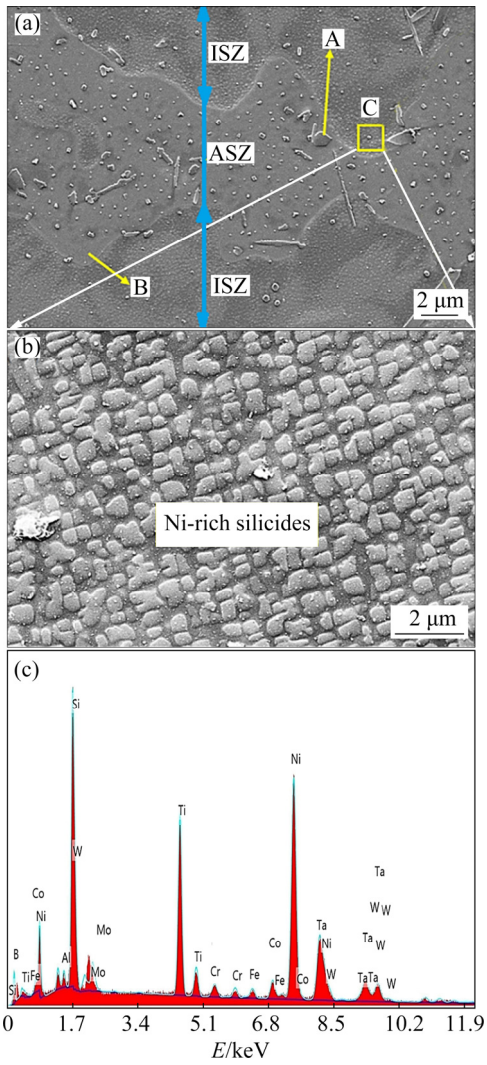

Fig. 8 FE-SEM micrographs of bond prepared using BNi-3 at 1100 °C for 1 min: (a) Eutectic structure containing Ni−Si−B intermetallics; (b) Ni-rich silicides; (c) EDS spectrum of Ni-rich silicides

Table 3 EDS analysis results of different areas in Fig. 8 (at.%)

Element	ISZ	ASZ		
	γ-solid solution	Ni-rich boride (Phase B)	Eutectic structure (Phase A)	Ni-rich silicide (Phase C)
Ni	76.65	72.94	74.71	70.41
Si	0.04	0.00	7.05	8.84
Cr	3.74	5.97	2.80	3.11
Ti	3.50	3.35	3.40	5.87
Nb	3.38	2.53	2.95	0.72
Fe	5.93	5.70	4.76	4.6
Co	1.27	1.28	0.68	1.71
Al	0.18	1.80	0.02	0.03
Ta	2.74	4.43	2.71	3.01
W	2.57	1.95	1.94	1.65

adjacent to the boride phase was observed. Because of the non-solubility of silicon in the boride phases, the concentration of silicon increases in the γ solid solution adjacent to the boride phases and a high concentration of Si could be recognized from the EDS study.

The results indicate that the ternary eutectic phase of a Ni-based solid solution phase, Ni-rich boride, and Ni-rich silicide was solidified because of the remaining liquid phase in the bonding centerline. The results of XRD analysis also confirm the presence of the phases mentioned above (Fig. 7(b)). Contrary to EDS results, as seen in Fig. 7(c), no silicide was detected in the ISZ microstructure, because of the Si content absence in the initial composition of BNi-9.

Assuming that the Point X in Fig. 9 is the chemical composition of the bonding zone, with a decrease of temperature in the γ phase area, nickel-rich solid particles begin to nucleate. According to the (a−a') dash line, the primary solid particles of Ni_3Si begin to nucleate. As the temperature decreases again, the amount of liquid decreases and its chemical composition moves toward the eutectic ternary point (E).

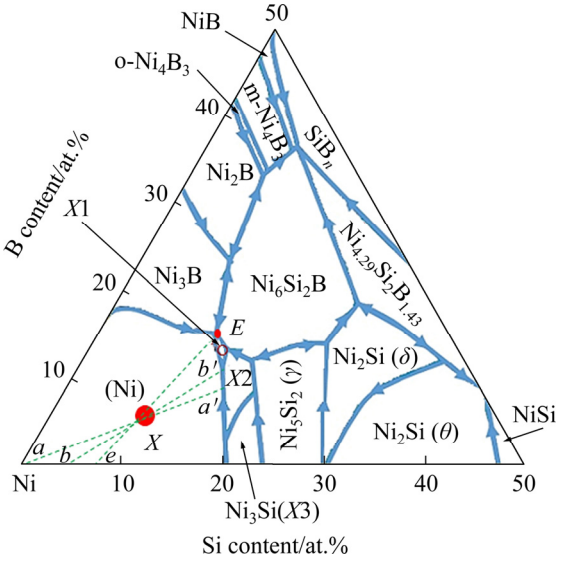

Fig. 9 Ternary phase diagram of Ni−B−Si [33]

Then, by changing the chemical composition of the liquid from a to b in Fig. 9, the amount of deposited Ni_3Si increases and moves towards the stable Ni_3Si region. Moreover, considering the b−b' line, it can be seen that by moving the liquid composition towards the eutectic composition, the γ and Ni_3Si amounts decreased and reached their maximum values at Point e. As can be seen in Fig. 8(b), in the primary stage of solidification, the size of Ni_3Si was small, and as the solidification progressed towards the eutectic composition, the size of the precipitation increased.

By moving from the liquid interface to the eutectic point, the Ni_3Si amount increased, leading to an increase in the size of Si-rich precipitates, but the precipitate size decreased in Region X. On the other hand, due to insufficient time for diffusion of the alloying element into the liquid and because of the formation of Si-rich precipitation (Ni_3Si) and Ni-rich phase in the remaining liquid, the remaining liquid is enriched with boron compounds. However, in this study, formation of Ni_6Si_2B was detected, as confirmed by the XRD patterns.

According to LEBRUN et al [33], the ternary eutectic reaction in Ni–Si–B can take place in two insignificantly different ways: $L \rightarrow \gamma + Ni_3B + \delta\text{-}Ni_6Si_2B$ in equilibrium conditions and $L \rightarrow \gamma + Ni_3B + \beta_3\text{-}Ni_3Si$ in metastable conditions. Accordingly, the solidification sequence can be summarized as follows [34]:

$$L \rightarrow \gamma + L \rightarrow \gamma + Ni_3B + L \rightarrow \gamma + Ni_3B + Ni_6Si_2B \quad (1)$$

3.1.3 Microstructure of joint using BNi-9 filler alloy

Figure 10(a) shows the typical microstructure of the bonding zone in the joints made with a BNi-9 interlayer at 1100 °C for 1 min. The result of the EDS analysis indicated that ISZ in the microstructure using BNi-9 rather than BNi-3 and BNi-2 is the same and consisted of Ni-rich solid solution. No silicide was detected in the ISZ microstructure, because of the Si content absence in the initial composition of BNi-9. The EDS results verified the absence of silicide in the ISZ microstructure. As can be seen in Fig. 10(a), the structural shape of the centerline region shows that the phases were formed through eutectic type reactions. The athermally solidified zone is composed of three distinct phases including: (1) Ni-rich borides, (2) Cr-rich borides, and (3) γ eutectics.

A wavy morphology shown in Fig. 10(b) suggests that the planar isothermal solidification front had changed into a cellular one. This is because of the presence of composition super-cooling in the process of non-isothermal solidification.

The EDS spectrum of ASZ illustrated in

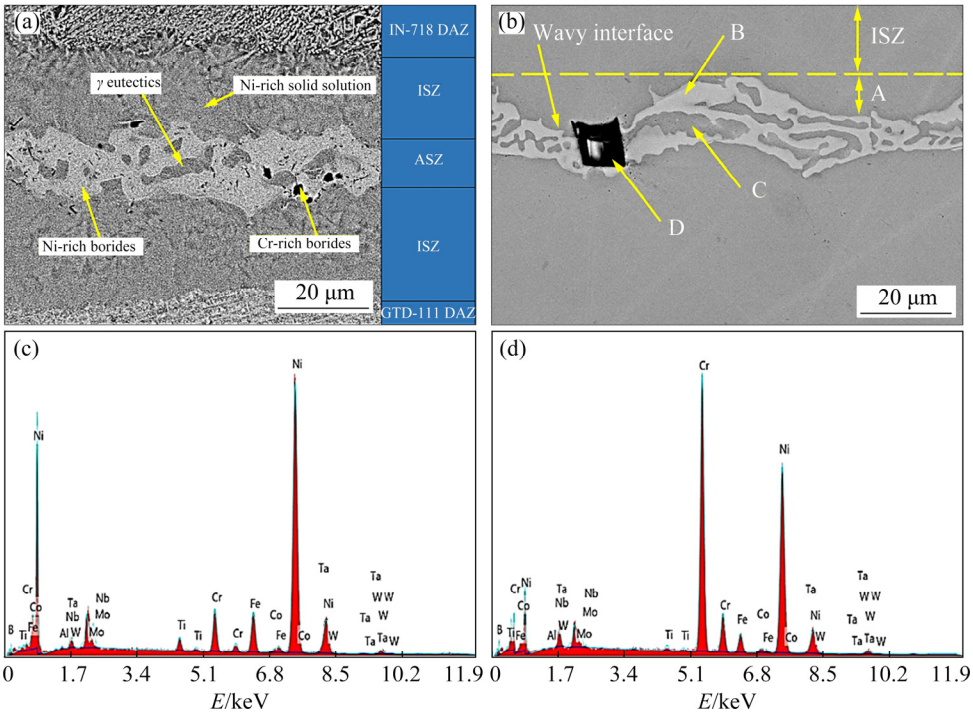

Fig. 10 Typical microstructures of bonding zone in joints made with BNi-9 interlayer at 1100 °C for 1 min: (a) ASZ microstructure of bond; (b) Wavy interface between γ phase and centerline intermetallics; (c) FESEM-EDS spectrum of Ni-rich boride phases (Zone B); (d) FESEM-EDS spectrum of Cr-rich boride phases (Zone D)

Figs. 10(c, d) suggests that these particles were Ni-rich borides and Cr-rich borides. The EDS analysis results (Table 4) and the corresponding EDS spectra depicted that the Regions A−D are most seemingly γ-proeutectics (γ-primary), Ni-rich boride, Cr-rich boride, and γ-eutectic phases, respectively. Although boron was detected in the Ni-rich boride, and Cr-rich boride phases by the ultrathin window EDS detector, quantitative determination of B could not be carried out with sufficient exactness by the EDS method. The existence of such phases was reported by IDOWU et al [35] and ARHAMI et al [36].

Figure 7(c) shows the XRD pattern of the GTD-1111/IN-718 joint using BNi-9 for 1 min, including the Ni and Cr-rich, and Ni matrix phases. The analysis of patterns by X'pert software reveals that Ni_3B, CrB, and the Ni matrix can be identified. Similar phases were reported in another study on the bonding of transient liquid phases with different interlayers [36].

3.2 Isothermal solidification completion time

The experimental results have shown that the isothermal solidification occurred after the bonding time of 60 min for BNi-2, after 45 min for BNi-3, and finally after 90 min for BNi-9 in the microstructural joint (Fig. 11). YUAN et al [37] evaluated the isothermal solidification rate of the TLP bonding of duplex stainless steel by two different Ni−B-based filler materials. They reported that boron diffusion at low temperatures and base metal alloying elements at high temperatures controlled the isothermal solidification rate.

Table 4 EDS analysis results of different areas marked in Fig. 10 (at.%)

Element	ISZ	ASZ		
	Ni-rich solid solution	Cr-rich borides	Ni-rich borides	γ-eutectics
Al	1.50	0.34	1.93	1.36
Nb	4.75	2.51	4.82	3.99
Mo	0.04	0.07	0.03	0.02
Ti	1.59	0.93	0.72	1.56
Cr	14.07	53.42	31.39	16.01
Fe	4.97	3.09	4.09	4.23
Co	1.38	0.74	1.04	1.48
Ni	67.64	37.01	53.84	69.87
Ta	2.07	1.32	1.28	1.00
W	1.98	0.56	0.86	0.47

POURANVARI et al [17] also reported that the bond microstructure and the isothermal solidification rate at a lower temperature are controlled by the diffusion of B and at higher temperature they are controlled by Nb diffusion during the dissolution of the base metal.

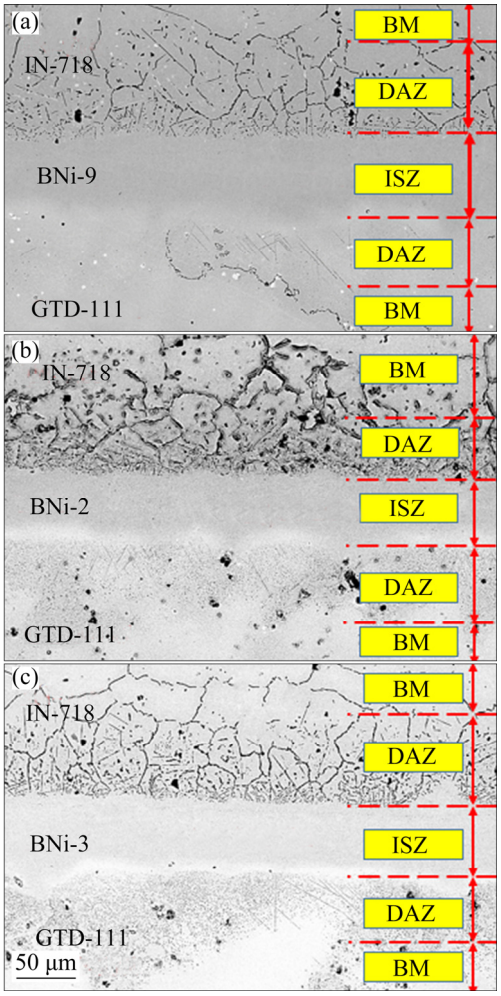

Fig. 11 Microstructures of TLP bonded IN-718/B−Ni compounds/GTD-111 system made at bonding temperature of 1100 °C after completion of isothermal solidification: (a) Bonding time of 90 min for BNi-9; (b) Bonding time of 60 min for BNi-2; (c) Bonding time of 45 min for BNi-3

According to Figs. 11(a, b, c), for bonding by the use of interlayer with different initial B, Si, and Cr contents, the eutectic free joints are concluded under the above-mentioned bonding conditions (1100 °C for three kinds of bonding time) and isothermal solidification completion takes place.

Studies have shown that differences in the concentration of B, Si, and Cr are the controlling elements for isothermal solidification of liquid using MBF-20 (BNi-2), MBF-30 (BNi-3), and MBF-80 (BNi-9), respectively [37]. As it has already been reported by YUAN et al [11], differences in the bond microstructure result from the Si and Cr contents and the bonding temperature. An increase in the enrichment of inter-diffusion alloy elements such as Ti and Al causes a decrease in the B solubility and this is the feasible reason for isothermal solidification rate.

3.2.1 Effect of B content on microstructure and isothermal solidification

It has been suggested that the filler metals with lower B content have a shorter isothermal solidification time. This means that increasing the initial B content of the filler metal extends the needed bonding time for the completion of isothermal solidification. By comparing experimental data among BNi-2, BNi-3 and BNi-9, it could be inferred that the completion of isothermal solidification using BNi-2, BNi-3 is faster than that using BNi-9. Estimation of isothermal solidification between BNi-2 and BNi-3 depends on the Cr content. POURANVARI et al [38] reported that there is a deviation for isothermal solidification time between the calculated results and experimental TLP bonding using BNi-9, BNi-3, and BNi-2 filler metals. It is important to consider the presence of B as insoluble inter-granular element in the highly alloyed BM of Ni-based super-alloys with the FCC γ-phase structure. B segregates at the grain boundaries of the base metal so that the base metal tends to have a brittle structure. The depletion of the base metal grain boundaries from Cr in Cr-borides might reduce the resistance of the base metal against corrosion and oxidation. Studies have shown that lower B content in an interlayer resulted in faster isothermal solidification compared to an interlayer with higher B content, but the Si effects on the isothermal solidification rate were not considered. SINCLAIR [39] showed that when we have a two-phase ternary system, a mechanism for the isothermal solidification stage is expected. When the diffusivities and/or solubilities of the two elements (B and Si) are significantly different, the solidification process is divided into two figurative systems: the first dominated by the faster diffusing element and the second dominated by the slower diffusing of the two [40]. In multicomponent transient liquid phase systems, the kinetics of solid/liquid interface movement is controlled by the faster element, which is boron in this case. B

diffusion into the base metals during bonding leads to the formation of borides due to the low solubility of the γ matrix for B and the presence of Cr, Mo, W, and Nb as strong boride forming elements.

3.2.2 Effect of Cr content on microstructure and isothermal solidification

The presence of Cr, as a strong boride former, can describe the formation of Cr-rich borides in the joint centerline. High values of the Gibbs free energy for Cr-rich borides formation can be regarded as the main driving force for their formation. This amount is −295.9 kJ/mol for Cr_3B_4 and −242.7 kJ/mol for Cr_3B_5 [13]. In the TLP process, when the B diffuses from the remaining melt through the isothermally solidified zone into the base metal, some Cr-borides will form. This means that the substantial Cr content might make an unpleasantly slow isothermal solidification rate. Based on the volume fraction of Cr in BNi-3 and BNi-9 filler alloy, we can conclude that the joint achieved using BNi-3 at 1100 °C for 45 min is free from the remaining liquid and the joint was obtained using BNi-9 (that is more Cr content than BNi-3) at 1100 °C for 90 min (Figs. 11(a, c)). Therefore, we could understand that because of the increase in the Cr content, the ASZ microstructure in the joint centerline with BNi-9 contains Cr-rich borides, Ni_3B, and Ni-rich solid solution. The effect of Cr was identified by YUAN et al [37] who reported that in the joint created at 1070 °C using MBF-80, ternary eutectic phases along the centerline region were obtained with increasing the Cr content in the filler after holding for the same time in contrast to MBF-30 and MBF-20. They showed that the Cr element might impede the relocation of B from the interlayer into the base metal.

As can be seen in Fig. 12(a), in the coupling of IN718 and GTD111 with BNi-2, it is possible to witness the effect that the inter-diffusion of Cr and/or Fe between the filler metal and IN-718 and inter-diffusion of Cr between the filler metal and GTD-111 have on TLP bonding, as it is well established that B diffusion away from the liquid phase is favored and that of Si is limited. Diffusion of Nb into the joint centerline of the IN-718 side and Ti and Ta into the joint centerline of the GTD-111 side was observed. It can be seen in Fig. 12(b) that the diffusion of B into GTD-111 and IN-718 results in preferential precipitation of Ni_3B.

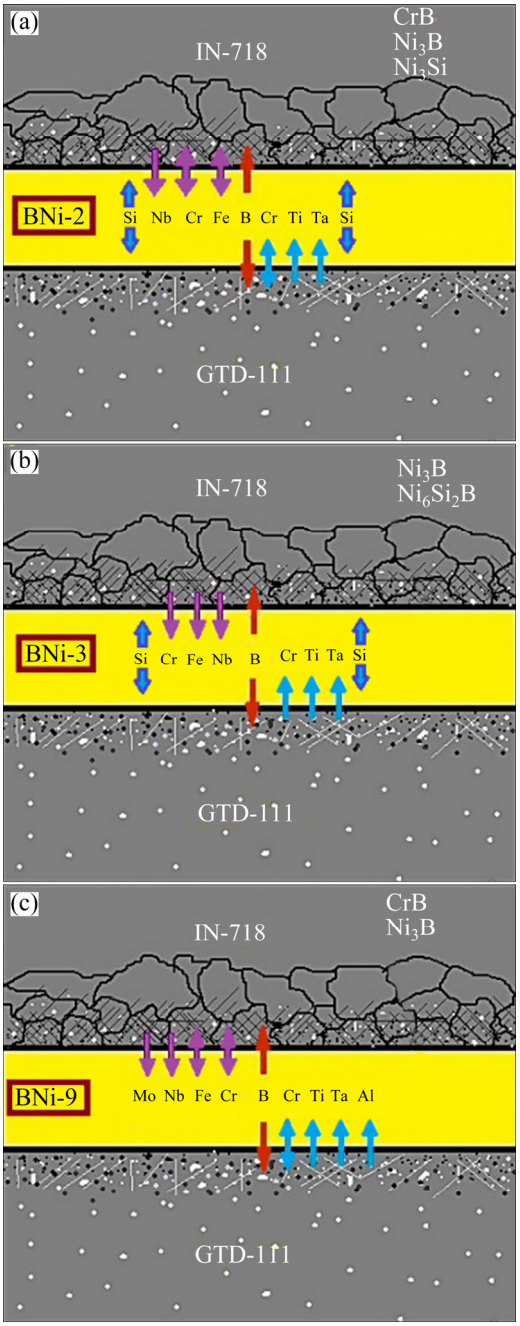

Fig. 12 Schematic representing possible solute transport mechanisms during evaluation of IN-718 and GTD-111 base metals with different filler metals: (a) BNi-2 (Ni−Cr−Fe−Si−B); (b) BNi-3 (Ni−Si−B); (c) BNi-9 (Ni−Cr−B)

Nevertheless, when adequate Cr is present (for example 13.5 wt.% Cr in GTD-111and 18 wt.% Cr in IN-718), Cr-rich borides are formed as controlled by equilibrium thermodynamics. In Fig. 12(c), it was determined that perceptible Cr depletion occurred within the DAZ region of IN-718, which could have impeded further precipitation due to an insufficiency of boride formers, e.g. Cr in GTD-111

and IN-718 as Cr_xB. When several boride phases were present, a Cr-rich boride was primarily formed within the grains similar to the morphology and composition reported for GTD-111. Also, Cr-rich boride which contained considerable concentrations of Ti, Ta, and Al precipitated preferentially not only on the grain boundaries of GTD-111 but also within the grains. For IN-718, additional Cr-rich boride contained substantial concentrations of Mo and Nb precipitated on the grain boundaries. Since the boride type (stoichiometry) is controlled by the substrate but is limited by Cr depletion, it was interesting to determine whether the filler metal containing Cr could reduce the depletion in such a way that the precipitation of borides was promoted.

3.2.3 Effect of Si content on microstructure and isothermal solidification

The high concentration of liquid from B and Si caused the shifting of the composition of the melt concerning ternary eutectic composition and formation of ternary eutectic products. In agreement with diagram phase of Ni−B−Si in Fig. 9, ternary eutectic reaction is $L \rightarrow \gamma + Ni_3B + Ni_6Si_2B$ [34]. Thus, the solidification sequence was summarized as Eq. (1).

The effect of the Si content on the isothermal solidification time is similar to that of the Cr content in the filler metal. This means that increasing the initial Si content of the interlayer prolongs the needed bonding time for the completion of isothermal solidification. In the ASZ of BNi-3 and BNi-2, Ni_3Si was detected but no Cr-boride phase was detected. Due to the small atomic size of boron (0.0079 nm) and essential diffusion of B into γ-Ni as an interstitial atom, a high diffusion rate can be achieved by B compared to Si [41]. In addition, BNi-3 and BNi-2 have a lower concentration of B with a significantly larger diffusion rate and higher Si content. But, in the BNi-9 interlayer, no silicide phase was detected while Ni_3B was detected. There are three reasons: (1) In BNi-9, the concentration of Si is low to exceed the solubility of Si in nickel silicide and γ-Ni; (2) There is a significantly larger partition coefficient of B in Ni (0.008) compared with the partition coefficient of Si in Ni (0.8); (3) In the condition of limiting the level of B, a ternary eutectic is not conformed. This is due to the non-sufficient volume fraction of borides for increasing the Si content in the remaining melt above the solid solubility limit in the nickel phase solid solution [38].

3.3 Mechanical properties

3.3.1 Bonding micro-hardness

Nickel-based interlayers are broadly used in brazing systems in the industry. Depending on the required physical and mechanical properties in the different industries such as joint melt temperature, melting-point range, strength, fluidity, economic cost, corrosion resistance, vapor pressure, ductility, and availability, we could use nickel-based filler metals.

Different micro-hardness values in the bond region and adjacent region made in various filler metals are shown in Fig. 13. The result depicts the

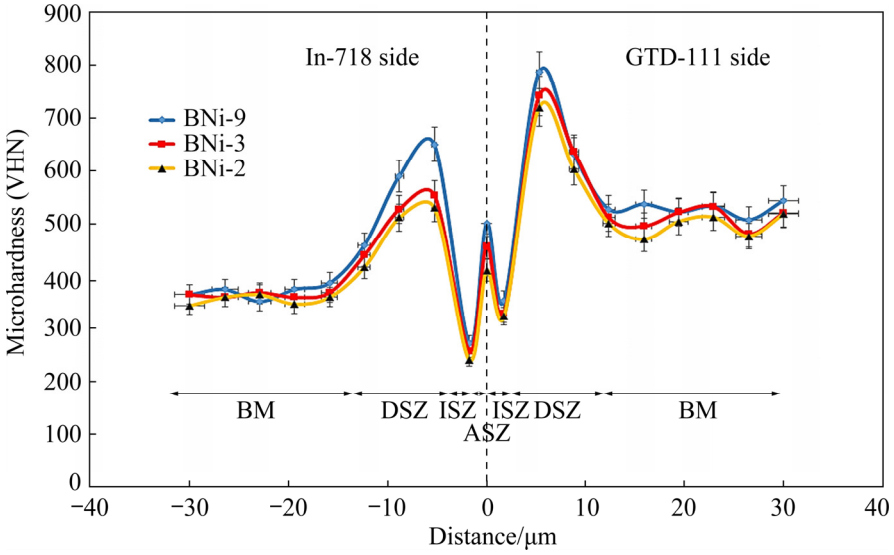

Fig. 13 Micro-hardness in bond region and adjacent region made with various filler metals

highest hardness in all of the samples is allocated to DAZ and then the ASZ region. The studies illustrate that increasing the concentration of some elements such as Al and Ti as γ' promoting elements in ISZ and Cr and Co as solid solution elements caused an increase in the micro-hardness of the phases [42]. As can be seen in Fig. 13, the highest hardness in the ASZ region belongs to BNi-9 and after that BNi-3 followed by BNi-2 which has the lowest hardness. The presence of higher B and Cr contents and the absence of Si content can be strong reasons for higher hardness of the BNi-9 interlayer in the ASZ region. By investigating Fig. 13, it can be inferred that differences in the hardness of three filler metals are appropriate ASZ and DAZ regions. It was shown that since the Ni-based filler metals contain no Si, such as BNi-9, the ultimate joining target can be achieved. The diffusion of B in the solid base metal is very fast; furthermore, with the migration of B from the joint to the solid base metal, the Cr borides are formed in the joint eutectic. In the filler metals having Si in addition to B, the B-free joints may have a strong and ductile solid solution matrix consisting of Ni, Si, and Cr elements after an extensive bonding time [43].

3.3.2 Bonding tensile shear strength

After the micro-hardness examination, the shear strength test of the dissimilar joint was done. The experimental results showed that the shear strengths of the joints by using BNi-9, BNi-2, and BNi-3 before the completion of isothermal solidification in the ASZ region are 305, 357, and 318 MPa, respectively. The shear strength of the joint using BNi-9 after the completion of isothermal solidification was higher compared with that using BNi-3 and BNi-2, which could be related to the absence of Si in the filler metal and the significant presence of Cr in BNi-9.

The shear strength of the joints bonded with different filler alloys at 1100 °C for 1 min is shown in Fig. 14(a). The experimental results showed that the shear strength of the TLP bonded joint has a direct relation with the hardness of ISZ of bonds. This means that non-isothermal solidification zones with hard intermetallic compounds have low shear strength and isothermal solidification zones that are free from the hard compounds have high shear strength and ductility.

Enhanced mechanical properties after the completion of isothermal solidification can be correlated to the ductile single phase γ solid solution formed in the bond area. Therefore, it can be concluded that higher hardness of the ISZ and lower hardness of the ASZ could result in higher joint shear strength.

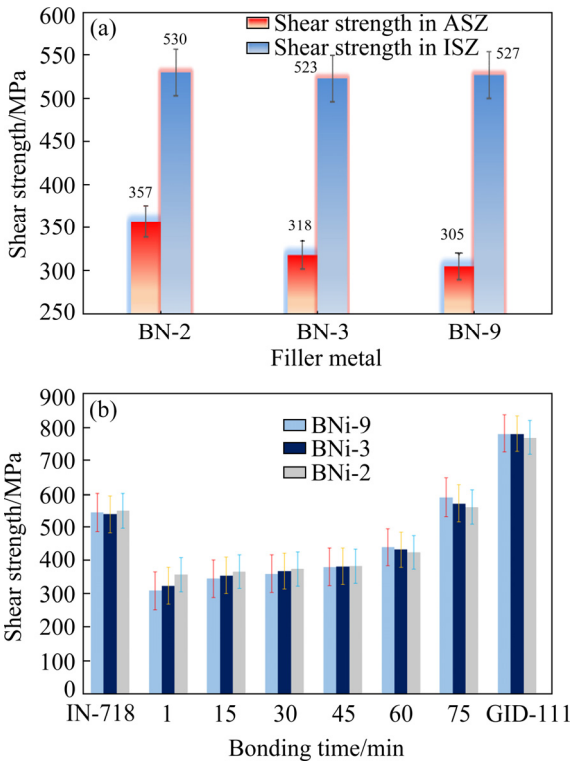

Fig. 14 Shear strength of joints bonded for different bonding time at 1100 °C: (a) In ASZ and ISZ regions; (b) Variety of shear strength of joints made using different interlayers with bonding time

The presence of Cr-rich boride phases increases the hardness of the joints. Therefore, the bonding made with the BNi-9 filler alloy, which has the highest value of these phases, has the highest value of hardness and, consequently, the lowest amount of shear strength. RABINKIN [13] showed that the joints with a high amount of Cr_3B have a low strength.

By increasing the bonding time to complete the isothermal solidification, the intermetallic compounds could be removed, which can cause an improvement of mechanical properties of the joint. It is believed that the bond shear strength increases with the holding time increment, as shown in Fig. 14(b). The relationship between shear strength and bonding time shows similar behavior at room temperature and 1100 °C. LIN et al [44] reported tensile−shear strength of the joints increases with

bonding time increasing at room temperature. With increasing the bonding time in different interlayers, it is observed that the shear strength increases from BNi-9 to BNi-2. This increment could be because of the major effective diffusion of the base metal alloying elements such as Cr into the filler alloy during a more prolonged bonding time and resulted from solid solution strengthening. Similar results were reported by POURANVARI et al [45]. Their results showed that various values of the shear strength are all lower than the value of the base metal.

SEM images of the fracture surface of the IN-718/GTD-111 TLP-bonded specimens at 1100 °C using BNi-2, BNi-3, and BNi-9 filler alloys are shown in Fig. 15. The SEM image displays crack and cleavage on the fracture surface. It is inferred that brittle fracture happened for the 1 min bonded joint due to the observation of the cleavage pattern on the flat fracture surface of this joint. Since the ratio of the ASZ to the ISZ is high in these samples, the appearance of the brittle fracture for these samples was assigned to the creation of the eutectic compounds into the bond region. These forms of fracture are named low-energy fractures which verify the weak shear strength of this bond [46]. As can be seen in Fig. 15, no dimple pattern was observed in the joints formed by different interlayers in 1 min bonding time. Consequently, the elimination of eutectic compounds could improve the shear strength of the joints. As it was mentioned before, due to the low shear strength in the bonding created with the BNi-9 filler alloy, the amount of the cleavage pattern is less than that with other interlayers and a pattern close to the dimple-shape is visible. The presence of cracks in the bonds also indicates the brittleness of the joints. According to Figs. 15(b, c), the amount of cleavage surfaces decreases in the bonding formed with BNi-3 and BNi-2, respectively. MALEKI et al [47] reported that the brittleness was due to the development of micro-cracks on the fractured surface. As it was previously mentioned, the highest micro-hardness belongs to the bonding formed by BNi-9, followed by BNi-3 and BNi-2 under the conditions of 1100 °C and bonding time of 1 min. Consequently, as shown in the fracture surface images (Figs. 15(a−c)), the greatest volume of cleavages and cracks belongs to BNi-3.

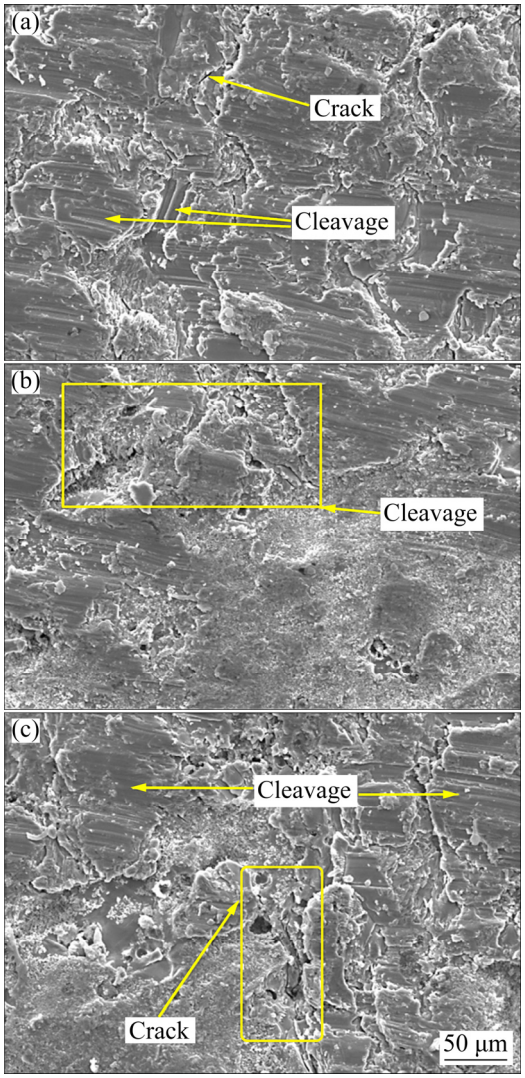

Fig. 15 Morphologies of fracture surface with different filler metals: (a) BNi-9; (b) BNi-2; (c) BNi-3

4 Conclusions

(1) Isothermal solidification, as the basic factor in obtaining intermetallics-free joint centerline, can be achieved after the bonding time of 60 min for BNi-2, after 45 min for BNi-3, and after 90 min for BNi-9 in the microstructural joint.

(2) In the case of the non-sufficient bonding time to complete isothermal solidification, the remaining liquid phase at the bonding temperature was converted into the non-equilibrium eutectic-type structure. This structure for BNi-2 and BNi-3 consists of γ-solid solution phase and boride and silicide phases and for BNi-9 consists of the γ-solid solution phase and boride phases. The formation of Ni_3B in the ASZ region is controlled by the B

content and, accordingly, the morphology of Ni_3Si is governed by the Si concentration. The Cr content might impede the relocation of B from the interlayer into the base metal and the formation of CrB inside the ASZ region is dominated by the Cr content.

(3) The decreased isothermal solidification rate could be assigned to the following reasons: the reduced concentration gradient in B between the base metal and the interlayer, the decreased B solubility, the enhanced Cr content in the filler metal, and the increased Si content in the insert alloy.

(4) The hardness profiles of the bonding zone revealed that the highest micro-hardness area is observed in ASZ, which is due to the existence of boride compounds such as brittle and hard nickel and chromium borides. The high micro-hardness of the eutectic compounds is originated from the formation of boride matrixes such as Ni or Cr boride. The shear strength of the joint using BNi-9 after the completion of isothermal solidification is lower compared that with BNi-3 and BNi-2, which could be related to the absence of Si in the filler metals constituent and the significant presence of Cr in BNi-9.

References

[1] POURANVARI M, EKRAMI A, KOKABI A. Microstructure development during transient liquid phase bonding of GTD-111 nickel-based superalloy [J]. Journal of Alloys and Compounds, 2008, 461: 641−647.

[2] DONACHIE M J, DONACHIE S J. Superalloys: A technical guide [M]. 2nd ed. ASM international, 2002.

[3] REED R, TAO T, WARNKEN N. Alloys-by-design: Application to nickel-based single crystal superalloys [J]. Acta Materialia, 2009, 57: 5898−5913.

[4] IDOWU O, RICHARDS N, CHATURVEDI M. Effect of bonding temperature on isothermal solidification rate during transient liquid phase bonding of Inconel 738LC superalloy [J]. Materials Science and Engineering A, 2005, 397: 98−112.

[5] OJO O, RICHARDS N, CHATURVEDI M. Study of the fusion zone and heat-affected zone microstructures in tungsten inert gas-welded INCONEL 738LC superalloy, [J]. Metallurgical and Materials Transactions A, 2006, 37: 421−433.

[6] OJO O, RICHARDS N, CHATURVEDI M. Effect of gap size and process parameters on diffusion brazing of Inconel 738 [J]. Science and Technology of Welding and Joining, 2004, 9: 209−220.

[7] DUVALL D S, OWCZARSKI W A, PAULONIS D F. TLP bonding: A new method for joining heat resistant alloys [J]. Welding Journal, 1974, 53: 203−214.

[8] BAKHTIARI R, SHAMSABADI A Y, MORADI K A. Shear strength/microstructure relationship for dissimilar IN738/IN718 TLP joints [J]. Welding in the World, 2020, 64: 219−231.

[9] GHAHFEROKHI A I, KASIRI-ASGARANI M, AMINI K, EBRAHIMI-KAHRIZSANGI R, RAFIEI M. Evolution of microstructure and mechanical properties on dissimilar transient liquid phase (TLP) bonding of GTD-111 and IN-718 by BNi-9 (AWS A5.8/A5.8M) interlayer [J]. Welding in the World, 2020, 65: 329−343.

[10] POURANVARI M. Solid solution strengthening of transient liquid phase bonded nickel based superalloy [J]. Materials Science and Technology, 2015, 31: 1773−1780.

[11] YUAN X, KIM M, KANG C. Effects of boron and silicon on microstructure and isothermal solidification during TLP bonding of a duplex stainless steel using two Ni−Si−B insert alloys [J]. Materials Science and Technology, 2011, 27: 1191−1197.

[12] BAKHTIARI R. Effect of configuration and composition of interlayer on TLP joints of FSX-414 superalloy [J]. Journal of Materials Processing Technology, 2016, 231: 8−17.

[13] RABINKIN A. Brazing with (NiCoCr)−B−Si amorphous brazing filler metals: Alloys, processing, joint structure, properties, applications [J]. Science and Technology of Welding and Joining, 2004, 9: 181−199.

[14] SILVA A L V C, MEI P R. Special steels and alloys [M]. 3rd ed. Sao Paulo: Blucher Publisher, 2010.

[15] DEVAUX A, NAZÉ L, MOLINS R, PINEAU A, ORGANISTA A, GUÉDOU J, UGINET J, HÉRITIER P. Gamma double prime precipitation kinetic in Alloy 718 [J]. Materials Science and Engineering A, 2008, 486: 117−122.

[16] SAJJADI S A, ZEBARJAD S M, GUTHRIE R, ISAC M. Microstructure evolution of high-performance Ni-base superalloy GTD-111 with heat treatment parameters [J]. Journal of Materials Processing Technology, 2006, 175: 376−381.

[17] POURANVARI M, EKRAMI A, AND KOKABI A. Diffusion brazing metallurgy of IN718/Ni−Cr−Si−B−Fe/IN718 [J]. Welding Journal, 2014, 93: 60−68.

[18] EGBEWANDE A, CHUKWUKAEME C, OJO O. Joining of superalloy Inconel 600 by diffusion induced isothermal solidification of a liquated insert metal [J]. Materials Characterization, 2008, 59: 1051−1058.

[19] SHAMSABADI A Y, BAKHTIARI R. TLP bonding of IN738/MBF20/IN718 system [J]. Journal of Alloys and Compounds, 2016, 685: 896−904.

[20] JALILVAND V, OMIDVAR H, RAHIMIPOUR M, SHAKERI H. Influence of bonding variables on transient liquid phase bonding behavior of nickel based superalloy IN-738LC [J]. Materials & Design, 2013, 52: 36−46.

[21] DANFLOU H L, MARTY M, WALDER A. Formation of serrated grain boundaries and their effect on the mechanical properties in a P/M nickel base superalloy [J]. Superalloys, 1992: 63−72.

[22] HOFFELNER W, KNY L, STICKLER R, MCCALL W. Effects of aging treatments on the microstructure of the Ni−base superalloy IN−738 [J]. Material Wissenschaft und Werkstofftechnik, 1979, 10: 84−92.

[23] SAJJADI S A, NATEGH S, GUTHRIE R I. Study of microstructure and mechanical properties of high performance Ni-base superalloy GTD-111 [J]. Materials Science and Engineering A, 2002, 325: 484−489.

[24] LEE H S, YOON J H, YOO J T, A study on tensile shear strength of IN 718 welded joint [J]. Advances in Materials and Processing Technologies, 2015, 1: 98−108.

[25] SOWA R, ARABASZ S, PARLINSKA-WOJTAN M. Classification and microstructural stability of high generation single crystal nickel-based superalloys [J]. Zaštita Materijala (Serbian), 2016, 57: 274−281.

[26] RUIZ-VARGAS J, SIREDEY-SCHWALLER N, GEY N, BOCHER P, HAZOTTE A. Microstructure development during isothermal brazing of Ni/BNi-2 couples [J]. Journal of Materials Processing Technology, 2013, 213: 20−29.

[27] NAALCHIAN M, KASIRI-ASGARANI M, SHAMANIAN M, BAKHTIARI R, BAKHSHESHI-RAD H R. Effect of substrate's heat treatment on microstructure and mechanical properties TLP bonding of dissimilar X-45/FSX-414 cobalt based superalloys [J]. Metals and Materials International, 2020: 1−12.

[28] CIESLAK M, STEPHENS J, CARR M. A study of the weldability and weld related microstructure of cabot alloy 214 [J]. Metallurgical and Materials Transactions A, 1988, 19: 657−667.

[29] YUAN X, KIM M B, KANG C Y. Characterization of transient-liquid-phase-bonded joints in a duplex stainless steel with a Ni−Cr−B insert alloy [J]. Materials Characterization, 2009, 60: 1289−1297.

[30] ARAFIN M, MEDRAJ M, TURNER D P, BOCHER P. Transient liquid phase bonding of Inconel 718 and Inconel 625 with BNi-2: Modeling and experimental investigations [J]. Materials Science and Engineering A, 2007, 447: 125−133.

[31] LEBAILI S, HAMAR-THIBAULT S. Liquid−solid balances in the Ni−B−Si system in the nickel-rich region [J]. Acta Metallurgica, 1987, 35: 701−710.

[32] BINESH B, GHAREHBAGH A J. Transient liquid phase bonding of IN738LC/MBF-15/IN738LC: Solidification behavior and mechanical properties [J]. Journal of Materials Science & Technology, 2016, 32: 1137−1151.

[33] LEBRUN N, PERROT P, SERBRUYNS A, TEDENAC J. Boron–nickel–silicon in refractory metal systems [M]. Berlin Heidelberg: Springer, 2010: 133−152.

[34] POURANVARI M, EKRAMI A, AND KOKABI A. Solidification and solid state phenomena during TLP bonding of IN718 superalloy using Ni−Si−B ternary filler alloy [J]. Journal of Alloys and Compounds, 2013, 563: 143−149.

[35] IDOWU O, OJO O, CHATURVEDI M. Microstructural study of transient liquid phase bonded cast Inconel 738LC superalloy [J]. Metallurgical and Materials Transactions A, 2006, 37: 2787−2796.

[36] ARHAMI F, MIRSALEHI S E, SADEGHIAN A, JOHAR M H. The joint properties of a high-chromium Ni-based superalloy made by diffusion brazing: Microstructural evolution, corrosion resistance and mechanical behavior [J]. Journal of Manufacturing Processes, 2019, 37: 203−211.

[37] YUAN X, KIM M B, KANG C Y. Microstructural evolution and bonding behavior during transient liquid-phase bonding of a duplex stainless steel using two different Ni−B-based filler materials [J]. Metallurgical and Materials Transactions A, 2011, 42: 1310−1324.

[38] POURANVARI M, EKRAMI A, KOKABI A. Diffusion induced isothermal solidification during transient liquid phase bonding of cast IN718 superalloy [J]. Canadian Metallurgical Quarterly, 2014, 53: 38−46.

[39] SINCLAIR C. Modeling transient liquid phase bonding in multicomponent systems [J]. Journal of Phase Equilibria, 1999, 20: 361.

[40] SINCLAIR C, PURDY G, MORRAL J. Transient liquid-phase bonding in two-phase ternary systems [J]. Metallurgical and Materials Transactions A, 2000, 31: 1187−1192.

[41] WU X, CHANDEL R, LI H. Evaluation of transient liquid phase bonding between nickel-based superalloys [J]. Journal of Materials Science, 2001, 36: 1539−1546.

[42] WILLEMIIN P, DURAND-CHARRE M. The nickel-rich corner of the Ni−Al−Ti system, [J]. Journal of Materials Science, 1990, 25: 168−174.

[43] RABINKIN A. Amorphous brazing foil at age of maturity [C]// Proceedings of the third International Brazing and Soldering Conference 2006. Sana Antonio, 2006: 1−9.

[44] LIN T S, LI H X, PENG H, XUE Y A N G, HUANG Y D, LIANG L I, LENG H A N. Effect of bonding parameters on microstructures and properties during TLP bonding of Ni-based super alloy [J]. Transactions of Nonferrous Metals Society of China, 2012, 22: 2112−2117.

[45] POURANVARI M, EKRAMI A, AND KOKABI A. TLP bonding of cast IN718 nickel based superalloy: Process–microstructure–strength characteristics [J]. Materials Science and Engineering A, 2013, 568: 76−82.

[46] HERTZBERG R W, VINCI R P, HERTZBERG J L. Deformation and fracture mechanics of engineering materials [M]. 6th ed. John Wiley & Sons, 2020.

[47] MALEKI V, OMIDVAR H, RAHIMIPOUR M R. Influences of gap size and cyclic-thermal-shock treatment on mechanical properties of TLP bonded IN-738LC superalloy [J]. Transactions of Nonferrous Metals Society of China, 2018, 28: 920−930.

中间层成分对 GTD-111/IN-718 高温合金在瞬时液相连接过程中显微组织和力学性能的影响

Ali IZADI GHAHFEROKHI[1], Masoud KASIRI-ASGARANI[1],
Kamran AMINI[2], Mahdi RAFIEI[1], Reza EBRAHIMI-KAHRIZSANGI[1]

1. Advanced Materials Research Center, Department of Materials Engineering, Najafabad Branch, Islamic Azad University, Najafabad, Iran;
2. Center for Advanced Engineering Research, Majlesi Branch, Islamic Azad University, Isfahan, Iran

摘　要：研究使用不同的中间层瞬时液相连接两种异种高温合金的适用性。在 1100 ℃、不同时间下瞬时液相连接 GTD-111/IN-718 体系，研究 BNi-2、BNi-3 和 BNi-9 三种类型的中间层对该体系显微组织和力学性能的影响。采用场发射扫描电子显微镜和能量色散光谱技术，研究接头区域的成分变化和显微组织。结果表明，非热凝固区 Ni_3B 的形成受 B 含量控制，相应地，Ni_3Si 的形貌受 Si 含量控制。Cr 含量可能会阻碍 B 从中间层向母材迁移，非热凝固区内 CrB 的形成主要受 Cr 含量的影响。硼化物如镍或铬硼化物基体的形成，使共晶化合物具有高的显微硬度。与使用 BNi-3 和 BNi-2 中间层的合金接头相比，等温凝固结束后，使用 BNi-9 中间层的合金接头其剪切强度更低，这可能与金属焊料成分中不含 Si 和 BNi-9 中含 Cr 有关。

关键词：瞬时液相连接；镍基高温合金；等温凝固；Ni−B 化合物

(Edited by Bing YANG)